Journal of Power Sources 609 (2024) 234709

Contents lists available at ScienceDirect

Journal of Power Sources

journal homepage: www.elsevier.com/locate/jpowsour

Waste minimization in all-solid-state battery production via re-lithiation of the garnet solid electrolyte LLZO

Vivien Kiyek [a,b,c], Martin Hilger [a,b,c], Melanie Rosen [a,c], Jürgen Peter Gross [d], Markus Mann [a,c], Dina Fattakhova-Rohlfing [a,c,e], Ruth Schwaiger [d,f], Martin Finsterbusch [a,c,g,*], Olivier Guillon [a,b,c,g]

[a] Institute of Energy and Climate Research – Materials Synthesis and Processing (IEK-1), Forschungszentrum Jülich GmbH, 52425, Jülich, Germany
[b] Institute of Mineral Engineering, RWTH Aachen University, Mauerstraße 5, 52064, Aachen, Germany
[c] Jülich-Aachen Research Alliance: JARA-ENERGY, 52425, Jülich, Germany
[d] Institute of Energy and Climate Research – Microstructure and Properties of Materials (IEK-2), Forschungszentrum Jülich GmbH, 52425, Jülich, Germany
[e] Faculty of Engineering and Center for Nanointegration Duisburg-Essen, University Duisburg-Essen, Lotharstr. 1, 47057, Duisburg, Germany
[f] Chair of Energy Engineering Materials, RWTH Aachen Univeristy, 52056, Aachen, Germany
[g] Helmholtz Institute Münster – Ionics in Energy Storage (IEK-12), Corrensstraße 46, 48149, Münster, Germany

HIGHLIGHTS

- Investigation of re-use of production waste of the solid electrolyte $Li_7La_3Zr_2O_{12}$.
- Waste powder and tape loses Li and thus forms a pyrochlore phases.
- A new processing route was developed to re-introduce the waste directly.
- The performance was shown to be almost identical to freshly synthesized powders.
- This approach minimizes waste of critical raw materials in future ASB production.

ARTICLE INFO

Keywords:
LLZO
Solid-state battery
Re-lithiation

ABSTRACT

Oxide-ceramic based electrolytes such as $Li_7La_3Zr_2O_{12}$ (LLZO), are one of the most promising solid electrolytes for application in all-solid-state batteries. However, most of its constituents are listed as critical raw materials, highlighting the need to minimize waste during synthesis and processing. Therefore, we investigated the re-use of aged LLZO powder and aged LLZO green foils produced by tape-casting, an industrial processing route suitable for ASSBs. We established a new synthesis route to fully recovery Li-poor LLZO and pyrochlore phase $La_2Zr_2O_7$ by simply adding a Li source during firing. By using recycled LLZO powder in a <200 μm thick cast tape, we were able to prove a similar ionic conductivity of 2.1×10^{-4} S cm^{-1} at room temperature and a critical current density of 0.75 mA cm^{-2} at 60 °C compared to fresh powder. This simple and efficient re-synthesis strategy might hold the potential to minimize waste streams of critical raw materials in future industrial production processes of solid-state batteries.

1. Introduction

Due to the environmental concerns raised by the production of battery raw materials, especially cobalt mining and lithium production, the European Union demands high recovery rates of 70–95 % for cobalt, nickel, copper, and lithium by 2030 in Li-Ion Batteries [1]. Recycling conventional Li-ion batteries has been thoroughly examined, resulting in the construction of a demonstrator plant [2]. The proposed approach combines existing recycling techniques from other industries, such as crushing, solvent extraction, hydrometallurgical-, and pyrometallurgical treatments, with newly developed methods, including robot-based disassembly [3] and deep eutectic extraction [4]. This approach

* Corresponding author. Institute of Energy and Climate Research – Materials Synthesis and Processing (IEK-1), Forschungszentrum Jülich GmbH, 52425, Jülich, Germany.
E-mail address: m.finsterbusch@fz-juelich.de (M. Finsterbusch).

https://doi.org/10.1016/j.jpowsour.2024.234709
Received 12 February 2024; Received in revised form 23 April 2024; Accepted 9 May 2024
Available online 14 May 2024

proved effective enough to meet the set goals for quantity. Nevertheless, the economic and environmental feasibility and the quality of the received materials must be further investigated and optimized. In addition to recycling discarded battery materials, direct reuse of these materials in manufacturing should also be considered, as this could lead to significant cost reductions [5–12].

Amongst new battery concepts, all solid-state batteries (ASSB) are attracting increasing interest. Within solid-state battery research, the oxide solid electrolyte $Li_7La_3Zr_2O_{12}$ (LLZO) has emerged as one of the most promising materials because of its stability against high-voltage cathodes and the lithium metal anode [13,14]. A well-established industrial process known as tape-casting produces LLZO separators for large-scale manufacturing. LLZO separators produced via tape-casting display sufficient ionic conductivity for full-cell production [15–21]. The obtained separators show critical current densities high enough to successfully suppress critical dendrite formation even at low thicknesses, enabling the production of LLZO-based ASSBs with competitive energy densities [19,20]. For solid-state batteries, recycling strategies should be developed simultaneously with the cells to ensure the lowest possible environmental impact and enable the integration of eco-design concepts. Therefore, waste generation during material production should be minimized, as LLZO not only uses rare earth elements, but its production is energy- and cost-intensive due to several high-temperature treatments at 1000 °C or above. For the material class of oxide solid electrolytes, possible processing routes for recovery of the metal oxides by dissolution were shown in a theoretical approach [22]. While the recycling of industry-relevant high-energy density cells has not been demonstrated thus far, the recovery of metal oxides from an LLZO-based solid-state battery has been shown [23]. Hydrometallurgical approaches were successfully used for selective leaching from LLZO powder, and LLZO sintered bodies using different acids [24]. Nevertheless, obtaining high-purity precursors for battery synthesis from recycling processes remains challenging, as the precipitation windows of the different ions are close.

Therefore, alternative strategies have been examined. One approach circumvents the decomposition of the valuable metal oxides by refurbishing the battery components, which minimizes costs as the energy-intense synthesis procedure does not have to be repeated. An example of refurbishment for conventional Li-ion cells has been successfully demonstrated with the extraction of cathode active material and the regeneration of $LiFePO_4$ (LFP) cathode active material [25,26]. This approach has also been transferred to sulfide-based lithium batteries, as specific sulfide electrolytes are soluble in water [27]. On the other hand, fully oxide-based solid-state batteries do not require extraction, and the direct regeneration of LLZO-LCO-based cathode-separator half-cells by heat treatment has been successfully demonstrated [28]. Still, industrially relevant ASSB concepts will combine different material classes, raising the need for solvent-based or thermal extraction processes to regain the cell components for refurbishment or recycling. Solvent-based extraction might be challenging for LLZO as it undergoes the Li^+/H^+-exchange [29], producing protonated LLZO with lower sintering activity and lower Li-ion conductivity. Combined with the lithium loss during high-temperature treatments, LLZO is expected to undergo phase changes and the development of secondary, lithium-poor pyrochlore phase $La_2Zr_2O_7$ during all hydrometallurgical and thermal extraction steps. Therefore, the reformation of phase-pure, cubic LLZO must be assumed as a critical step during the refurbishment of LLZO-based battery components.

A post-lithiation of $La_2Zr_2O_7$ has already been successfully demonstrated for ultra-thin films by the PLD (pulsed laser deposition) process (up to 110 nm) [30]. For thicker LLZO components, the influence of the atmosphere flow and lithium loss on forming the LLZO phase has already been investigated [31]. Therefore, to overcome a lithium-poor $La_2Zr_2O_7$ phase formation and compensate for lithium loss, lithium excess is usually added during the synthesis of LLZO. This excess lithium has been demonstrated to play a critical role in the processability and electrochemical performance of the produced components [15].

In this work, we first look into refurbishing both LLZO waste powder and battery components waste, which would be a real application case in a factory producing separators or oxide-based cells. We successfully reuse lithium-depleted LLZO by controlling the sintering activity and atmosphere. The produced LLZO separators from waste material display suitable ionic conductivity ($>1 \times 10^{-4}$ S cm^{-1}) and dendrite stability (0.75 mA cm^{-2}), able to compete with pristine separators.

2. Materials and methods

Two main waste material streams have been identified for the recycling of LLZO (Fig. 1). The first consists of pure, aged $Li_{6.4}La_3Zr_{1.6}Ta_{0.4}Al_{0.05}O_{12}$ (LLZO:Ta,Al) powder, e.g., from powder leftovers, possibly out-of-spec products and will further be named LLZO-p. The second consists of aged LLZO:Ta,Al powder mixed with organics, e.g., from tape cut-offs after heat treatment, and will be named LLZO-t. Since industrial production of LLZO-based batteries has not been in place, model materials have been produced to test the refurbishing processes adequately.

2.1. Sample preparation

For the production of the LLZO-p material, LLZO powder has been prepared for the tape-casting process as described in our previous work via solid-state reaction [15]. Afterwards, the powder was stored in air for four months. The powder was heat-treated at 750 °C for 2 h in air for up to 2 times during storage. This heat treatment simulates a failure in LLZO synthesis or mimics the failure after processing some parts of LLZO powder already to battery material, as a heat treatment is subsequently needed to reverse the Li^+/H^+-exchange present in LLZO material [32]. This results in lithium loss and the formation of protonated LLZO [29], as well as lithium-poor secondary phases. Green tapes have been produced to produce of the LLZO-t material described in a previous work [15]. The green tape waste with varying storage times (up to four months) has been manually crushed and mixed homogeneously. To recover pure LLZO-t powder without organic from the green tapes, the crushed tapes were placed in an Al_2O_3 crucible with a closed lid and heated to 600 °C for 2 h in air to burn out the organic components. The exact heating profile can be found in Fig. S1. The de-bindered powder was milled in ethanol using ZrO_2 milling balls and jar at 500 rpm for 250 min in a planetary ball mill (Pulverisette 7 premium, Fritsch) to again obtain particle sizes suitable for tap-cast slurries. Afterwards, the powder was dried in air at 80 °C for 8 h.

All green tapes were produced using the same recipe, which can be found elsewhere [15]. The resulting green tapes were sintered in closed Al_2O_3 crucibles on an LLZO powder bed. Smaller Al_2O_3 crucibles filled with varying amounts of Li_2CO_3 were placed inside the sintering crucibles alongside the samples. For LLZO-p, the concentration of LLZO:Li_2CO_3 by mass was 1:0.55; for LLZO-t samples, the ratio was 1:2.22. All samples were sintered at 1185 °C for 24 h with heating and cooling rates of 5 K min^{-1}.

2.2. Structural characterization

To obtain information about the samples' phase purity and crystal structure, we performed X-ray diffraction (XRD) measurements. The instrument was a Bruker D4 Endeavour instrument using Cu-Kα radiation and equipped with a 1D detector LYNXEY and a DIFFRACplus BASIC package, which was released in 2009. All samples were measured from 10° to 80° 2Θ with 0.02° steps. The particle size distribution (Fig. S2) of the LLZO-p, LLZO-t before and after milling was checked via laser diffraction using an LA950 (Horiba Scientific) with a 650 nm and a 405 nm laser source; data were analyzed via Mie-theory. The pristine LLZO powder, and sintered tapes of LLZO-p and LLZO-t were crushed to powder to analyse the stoichiometry with Inductively coupled plasma

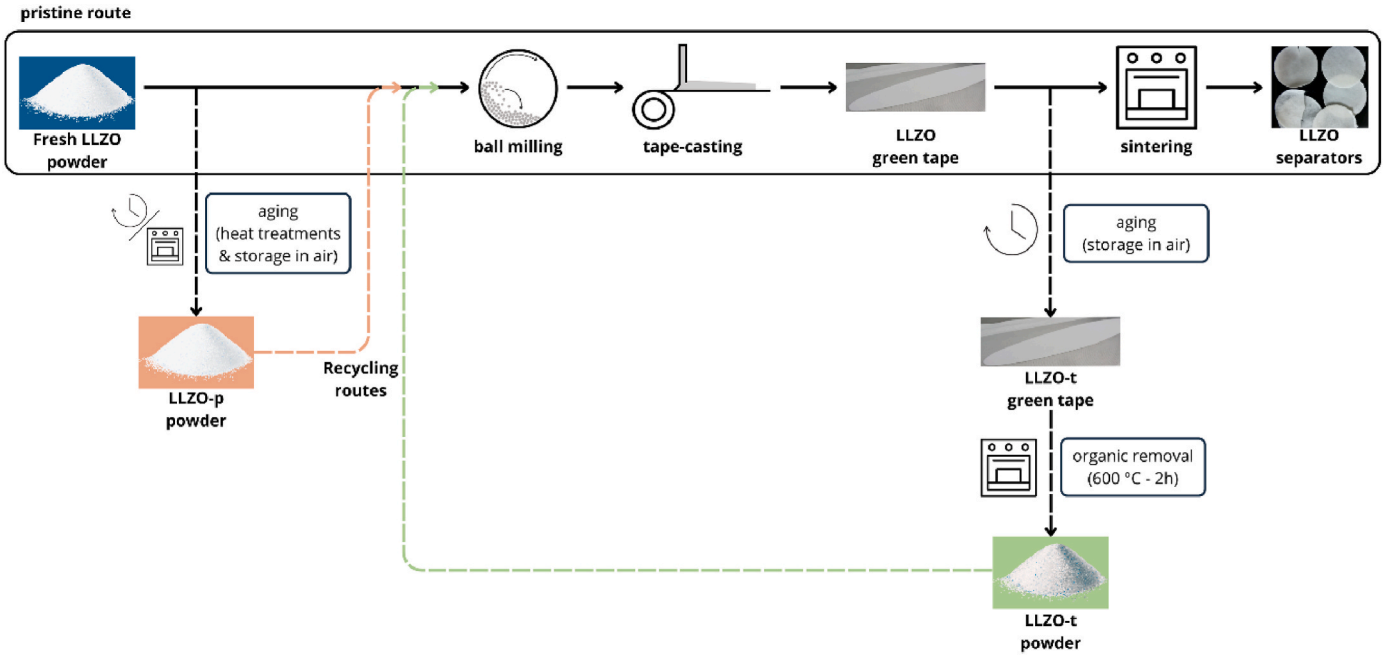

Fig. 1. Overview of the origin of LLZO-p and LLZO-t powder for recycling strategies.

optical emission spectroscopy (ICP-OES).

The sintered specimens were cut in half and embedded in epoxy resin for the microstructural characterization of the cross-sections. The cross-sectional surfaces were ground with SiC grinding paper and polished with water-free diamond suspension. After final polishing, the cross-sectional surfaces were prepared by Ar-ion milling (3 kV acceleration voltage, 380 μA discharge current) using a flat milling system (IM-3000, Hitachi). A thin iridium layer was sputtered onto the sample surface to compensate for charging effects (Q150TS coater, Quorum). Scanning electron microscope (SEM) images were taken using a field emission scanning electron microscope (Merlin, Carl Zeiss Microscopy) equipped with the X-Max Extreme EDX-detector (Oxford Instruments). Porosity estimations were carried out based on the analysis of SEM images using ImageJ [33], grain size distribution was measured manually in the same software by counting 500 grains over the total thickness of the tape.

2.3. Electrochemical characterization

For electrochemical characterization, the obtained separators were heated in argon for 2 h at 750 °C to remove Li_2CO_3 from the surface that forms during contact with ambient air. The clean surface ensured a comparable interface for the electrochemical characterization; details of this procedure can be found elsewhere [34]. Symmetrical Li|LLZO|Li cells were assembled under an argon atmosphere. A thin gold interlayer was sputtered onto the sample surface (~30 nm, Cressington 108 auto Coater), and as-calendared metallic lithium was manually pressed on each side. The half-cell was then placed between two Ni-discs and heated to 300 °C for 2 min to ensure good contact. After cooling to room temperature, the sample was transferred to a Swagelok cell, sealed, and removed from the glovebox to perform electrochemical tests. Using a BioLogic VMP-300 multi-potentiostat, the impedance of the pellets was measured at room temperature, and the resistance and conductivity were extracted. The frequency was varied from 7 MHz to 1 Hz with an electrical field perturbation of 10 mV. To investigate dendrite formation, impedance and critical current density (CCD) measurements were conducted at 60 °C using the same multi-potentiostat. The lithium was stripped and re-plated for this test at an increasing current density. It started from 5 μA (9.94 μA cm^{-2}) for 30 min per step with an increment of 5 μA per cycle for LLZO-t measurement, while for LLZO-p reaching 50 μA (99.4 μA cm^{-2}), the increment was increased by 15 μA per cycle instead of 5 μA. Here, the critical current density is defined to be reached when the first Li dendrite grows by observing a significant voltage drop.

3. Results and discussion

XRD analysis of the materials LLZO-t and LLZO-p show significant changes compared to the pristine materials (Fig. 2 a and **b**). For LLZO-t, pristine materials were used for tape-cast and analysis, shown somewhere else [15]. LLZO-p pristine powder is used for either water-based tape-cast or pellet pressing and sintering (conventional and via Field-Assisted Sintering Techniques (FAST)), and the results are shown elsewhere. [16,35–37]. LLZO-p has formed a secondary $La_2Zr_2O_7$ phase during pre-treatment, which typically appears after high-temperature decomposition of LLZO [38] but can also be observed at lower temperatures after prolonged heat treatment with insufficient lithium excess. Similarly, LLZO-t shows significant amounts of $La_2Zr_2O_7$ secondary phase, and Li_2CO_3 due to the additional Li^+/H^+-exchange during wet-processing in the tape-casting process. After removing organic additives from the green tape waste by the heat treatment (see Supplemental Fig. S1), the received LLZO-t powder consists only of $La_2Zr_2O_7$ with minor peaks of Li_2CO_3 present in the XRD. The received powder was wet-milled in ethanol to re-adjust the particle size to a range suitable for tape-casting (see Supplemental Fig. S2).

LLZO-t and LLZO-p powders were used in a tape-casting process without further treatment. The process is, therefore, similar to freshly synthesized LLZO separators via a tape-casting process, except for the additional lithium source during firing. For LLZO-p samples, sintering led to the reformation of cubic LLZO with minor peaks for Li_2CO_3. The minor peaks can be attributed to the Li^+/H^+-exchange during cooling of the samples in ambient air (Fig. 2 a and **b**). In contrast, LLZO-t required a higher concentration of lithium atmosphere for full lithiation. Still, phase pure cubic LLZO was obtained, even though previously, the primary phase in the LLZO-t waste was $La_2Zr_2O_7$. We suggest is that the pyrochlore phase as $La_2Zr_2O_7$ undergoes a second formation step of LLZO. It is known that during the formation of LLZO, $La_2Zr_2O_7$ will be formed already around 400 °C, with its maximum amount shortly before 800 °C and then with the existing Li-source (which can be either Li_2CO_3 or LiOH) forms LLZO. [39,40]. Furthermore, ICP-OES (Inductively

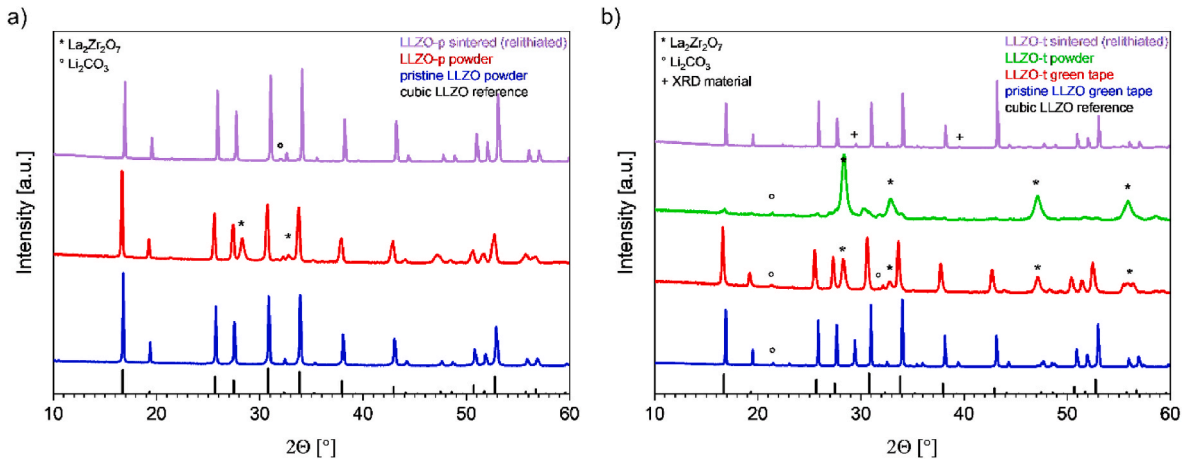

Fig. 2. a) XRD data of pristine LLZO powder, LLZO-p powder and LLZO-p sintered tapes, which show recovery of the cubic LLZO structure in the sintered tapes, while **b)** shows XRD data of pristine LLZO green tape, LLZO-t tape, LLZO-t powder after heat-treatment with no cubic LLZO structure and LLZO-t sintered tapes showing a recovery of the cubic LLZO structure. Both figures have a cubic LLZO reference demonstrated in black [ICSD:182,312] [42]. (For interpretation of the references to colour in this figure legend, the reader is referred to the Web version of this article.)

coupled plasma optical emission spectroscopy) measurements were performed to evaluate the chemical lithiation between recycled tapes and the pristine powder (see Supplementary Table S1). The measured stoichiometry deviates in a systematic manner from the expected stoichiometry due to specific issues with LLZO during ICP measurements [41]. However, due to the systematic nature, a direct comparison between the three samples is still possible. Pristine LLZO matches the recycled values within the error, except for the Al value. Here, an uptake of the Al can be seen in the LLZO-t and LLZO-p tapes. Such an Al uptake is known to originate from the sinter crucible during heat treatment, and thus cannot be found in the pristine powder as it was not sintered to a tape. Overall, this proves the effectiveness of the recycling approach presented here to re-lithiate the structure and obtain material that is close to the original stoichiometry.

This shows that Li-poor LLZO and $La_2Zr_2O_7$ can be converted to phase-pure LLZO by adjusting the Li excess in the sintering atmosphere. The new method paves the way for straightforward integration into industrial waste processing, thus reducing waste generation effectively. Nevertheless, industrial feasible processes tailored to all-solid-state batteries must still be developed, especially for oxide-based solid electrolytes. In particular, there are various challenges for the direct transfer of industrial LIB recycling to ceramic-based cells. On the one hand, the hard nature of oxide-ceramics can lead to difficulties in pre-processing, e.g. during comminution, leading to faster wear of the equipment. On the other hand, during re-introduction into the original process stream, optimization might be possible to adapt to a certain amount of recycled material in “fresh” material, which is a common practice in many recycling applications on industrial level. While tape-casting is an established industrial process, the casting and sintering of LLZO based separator-tapes, still needs to be verified on an industrial level and was thus not attempted in this paper. However, this fact makes it even more obvious that simplified recycling approaches for oxide-based all-solid-state batteries are urgently needed so adaptation can start early and will be more straightforward.

Flat, sintered LLZO separators with a thickness between 175 μm and 190 μm were obtained from green tapes of both LLZO-p and LLZO-t powders. Due to the slight differences in particle size distribution (PSD), slurries vary slightly, resulting in different heights of green and sintered tapes (see Supplemental Fig. S2). SEM pictures were taken of the embedded and polished cross-section of the solid electrolytes produced from LLZO-p and LLZO-t tapes after electrochemical testing and removing the lithium anode in a glovebox. The polished cross-section was used to visually determine the relative density of the sample and manually evaluate the grain size distribution. The produced separators show small and large pores and an overall relative density of approximately 87 % (Fig. 3 a). LLZO-p tapes show significant grain growth (Fig. 3 c), with grain sizes reaching values higher than 15 μm. By contrast, the polished cross-section of the sintered LLZO-t tapes after electrochemical testing (Fig. 3 b) reveals less densification of approximately 76 % even after sintering with the highest lithium concentration in the atmosphere. The grain size is smaller overall than that of LLZO-p tapes. Low densification indicates insufficient sintering activity of the LLZO-t material, which might be due to a high average particle size distribution after milling (see Supplemental Fig. S2).

The electrochemical performance of the sintered separators for both LLZO-t and LLZO-p was determined by building symmetrical Li|LLZO|Li half cells. The free-standing separators cannot be polished without breaking due to the reduced thickness of under 200 μm and the brittle nature of the ceramic electrolyte. The separator surface was therefore cleaned from Li_2CO_3 by heating the separators in argon [15]. A gold interlayer sputtered onto the LLZO surface and heated with the metallic lithium to form an alloy and to ensure intimate contact between the lithium metal and the rough separator surface [43].

Impedance measurement of the cells containing the LLZO-t separators reveals three semi-circles at room temperature. The bulk conductivity of LLZO cannot be distinguished in the investigated frequency range (Fig. 4 a and b). The grain boundary resistance is determined as 95 Ω with a capacitance of 10^{-9} F, followed by the resistance of the lithium interface (10^{-4} F). From this, the ionic conductivity of the LLZO-t separator is determined as 1.4×10^{-4} S cm^{-1} at room temperature. Despite these comparably good values, the critical current density during plating and stripping the symmetrical Li|LLZO|Li cell is only around 110 μA cm^{-2} at 60 °C (Fig. 5 a). These findings correspond to the microstructural characterization, as low density decreases the dendrite stability of the separator significantly. For recycled LLZO with such severe de-lithiation, the proposed one-shot refurbishing process must be replaced with a separate relithiation step to reform LLZO before component production.

Impedance measurements of the LLZO-p separators (Fig. 4 c and d) show lower room temperature resistances, with a grain boundary resistance of 47 Ω (10^{-7} F). At room temperature, the ionic conductivity is determined as 2.1×10^{-4} S cm^{-1}. In contrast to the LLZO-t separators, the separators obtained from the LLZO-p powder display outstanding dendrite resistance. The critical current density is 750 μA cm^{-2} at 60 °C (Fig. 5 b).

Compared to similar processed LLZO tapes from pristine powder, they show relative densities up to 92.8 % (here 87 %), conductivity at room temperature at 3.9×10^{-4} S cm^{-1} (here 2.1×10^{-4} S cm^{-1}) and a

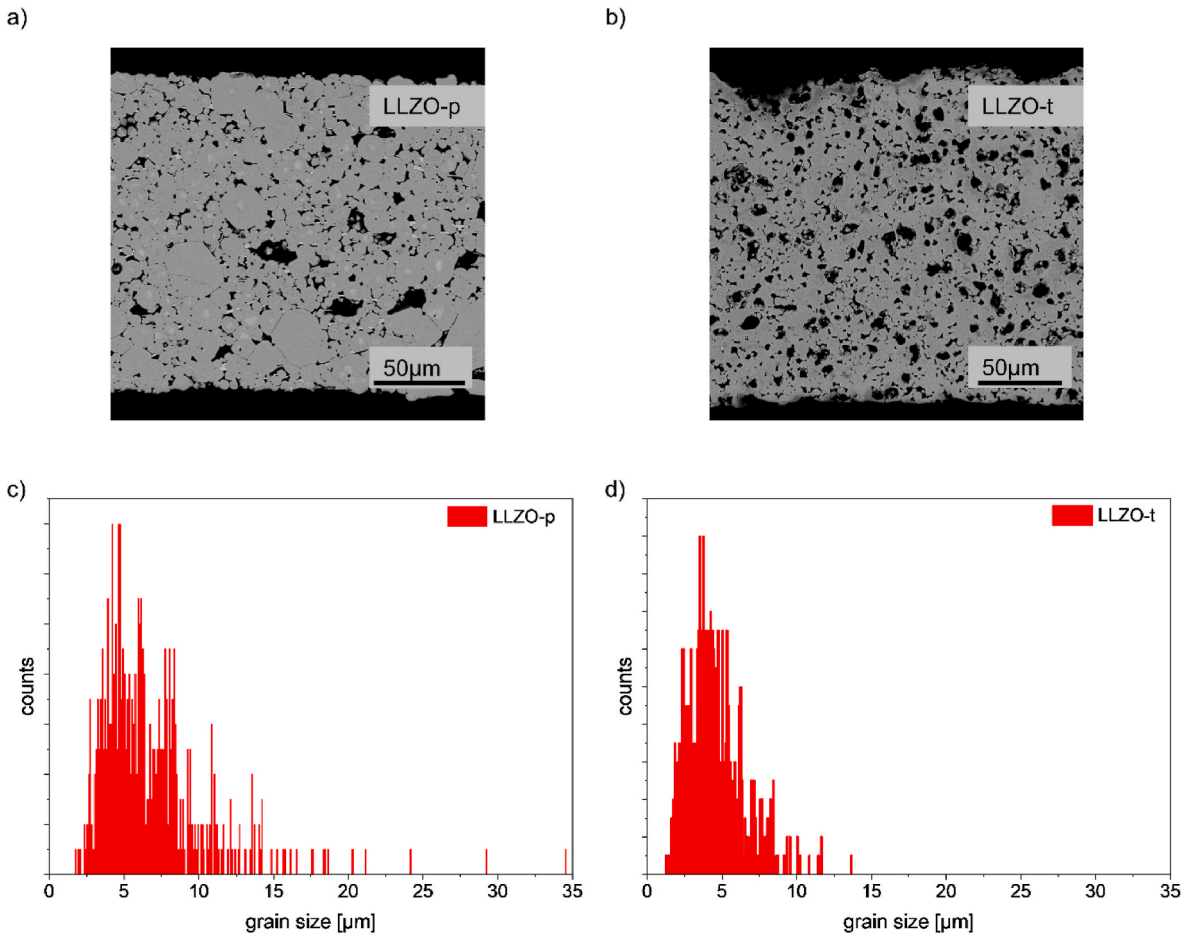

Fig. 3. a) SEM image of a polished cross-section of LLZO-p after sintering and electrochemical testing, Li anode was removed carefully, while **b)** shows SEM image of a polished cross-section of LLZO-t after sintering and electrochemical testing, with a higher visual porosity. **C)** and **d)** show grain size distribution of 500 grains measured manually from the SEM pictures of LLZO-p and LLZO-t, respectively.

critical current density with 318 µA cm^{-2} at 50 °C (here: 750 µA cm^{-2} at 60 °C) [15]. This proves the feasibility of the presented refurbishing process for low and moderate de-lithiation of the refurbished LLZO material and marks the highest critical current density of a tape-cast LLZO separator so far. However, the temperature is different and highly influences the critical current densities; comparability must be taken carefully.

4. Conclusions

In this work, we have introduced model materials for recycling LLZO solid electrolyte material from recycling production waste. A novel, easy, one-step refurbishing method was introduced. We highlight the delicate balance between the lithium shortage in the spent or recovered material and the suitable refurbishing conditions. The combination of sintering intensity and Li-enrichment influences densification, grain growth, and grain boundary properties, governing the electrochemical performance of the obtained separators. LLZO separators with a competitive ionic conductivity of 2.1 × 10^{-4} S cm^{-1} at room temperature and outstanding critical current densities of 750 µA cm^{-2} at 60 °C have been obtained for low and moderate lithium-loss. For high lithium loss from LLZO green tape waste, LLZO separators with slightly lower ionic conductivity have been obtained. Even though this procedure is not yet optimized for green tape waste, this approach represents an efficient way to minimize LLZO waste streams with in-situ processes by adding an additional lithium source.

Funding

This research was funded within the project "S2taR—Development of All-Solid-State Battery Recycling Processes" (grant numbers 03XP0319C) of the Competence Cluster Recycling & Green Battery (greenBatt) and the project "FB2-Oxide" (grant number 13XP0434A) of the Cluster FestBatt2.

CRediT authorship contribution statement

Vivien Kiyek: Writing – review & editing, Writing – original draft, Visualization, Validation, Supervision, Investigation, Formal analysis, Data curation, Conceptualization. **Martin Hilger:** Validation, Investigation, Data curation. **Melanie Rosen:** Writing – review & editing, Writing – original draft, Validation. **Jürgen Peter Gross:** Writing – review & editing, Methodology, Investigation. **Markus Mann:** Writing – review & editing, Writing – original draft, Methodology. **Dina Fattakhova-Rohlfing:** Writing – review & editing, Supervision. **Ruth Schwaiger:** Writing – review & editing, Supervision. **Martin Finsterbusch:** Project administration, Funding acquisition, Conceptualization. **Olivier Guillon:** Writing – review & editing, Project administration, Funding acquisition, Conceptualization.

Declaration of competing interest

The authors declare that they have no known competing financial interests or personal relationships that could have appeared to influence

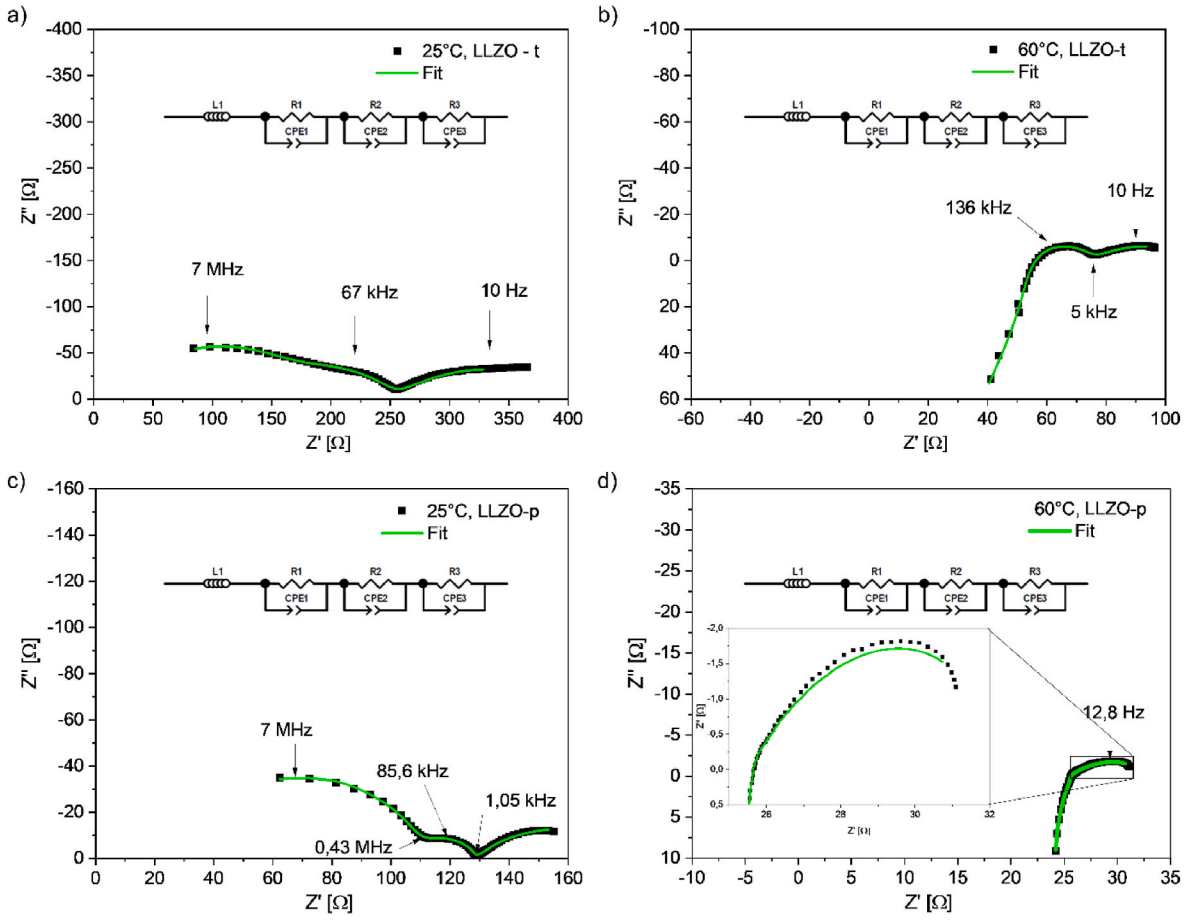

Fig. 4. Electrochemical Impedance Spectroscopy of symmetrical Li|LLZO|Li cells. While **a)** and **b)** show the spectra of the LLZO-t sample measured at 25 °C and 60 °C, respectively, reaching a total ohmic resistance of <375 Ω (<100 Ω, respectively) **c)** and **d)** show the spectra of LLZO-p sample measured at 25 °C and 60 °C, respectively, reaching a total ohmic resistance of <160 Ω (<35 Ω, respectively).

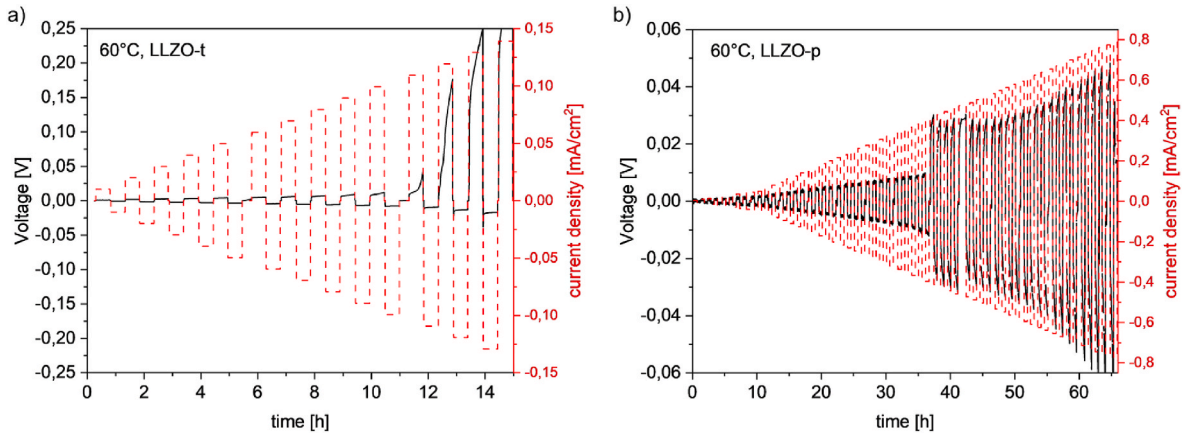

Fig. 5. CCD measurement on a symmetrical Li|LLZO|Li cell at 60 °C of **a)** LLZO-t and **b)** LLZO-p. Red and black lines indicate applied current density and change in cell polarization, respectively. CCD has been reached, when voltage drops, polarization is not considered. (For interpretation of the references to colour in this figure legend, the reader is referred to the Web version of this article.)

the work reported in this paper.

Data availability

Data will be made available on request.

Acknowledgments

The authors would like to thank Grit Häuschen for initial LLZO powder synthesis, Andrea Hilgers for the help with PSD analysis and Volker Bader for the heat treatments and ZEA-3 fot ICP-OES measurements.

Appendix A. Supplementary data

Supplementary data to this article can be found online at https://doi.org/10.1016/j.jpowsour.2024.234709.

References

[1] Regulation of the European Parliament and of the council concerning batteries and waste batteries, Repealing Directive 2006/66/EC and Amending Regulation (EU) No 2019/1020, 2020.
[2] A. Kwade, J. Diekmann (Eds.), Recycling of Lithium-Ion Batteries. The LithoRec Way, Springer, Cham, 2018.
[3] R. Gerbers, K. Wegener, F. Dietrich, K. Dröder, in: A. Kwade, J. Diekmann (Eds.), Recycling of Lithium-Ion Batteries. The LithoRec Way, Springer, Cham, 2018, pp. 99–126.
[4] M.K. Tran, M.-T.F. Rodrigues, K. Kato, G. Babu, P.M. Ajayan, Nat. Energy 4 (2019) 339–345.
[5] J. Chen, Q. Li, J. Song, D. Song, L. Zhang, X. Shi, Green Chem. 18 (2016) 2500–2506.
[6] M.J. Ganter, B.J. Landi, C.W. Babbitt, A. Anctil, G. Gaustad, J. Power Sources 256 (2014) 274–280.
[7] H.S. Kim, E.J. Shin, Bull. Kor. Chem. Soc. 34 (2013) 851–855.
[8] X. Li, J. Zhang, D. Song, J. Song, L. Zhang, J. Power Sources 345 (2017) 78–84.
[9] Y. Shi, G. Chen, Z. Chen, Green Chem. 20 (2018) 851–862.
[10] S. Sloop, L. Crandon, M. Allen, K. Koetje, L. Reed, L. Gaines, W. Sirisaksoontorn, M. Lerner, Sustainable Materials and Technologies 25 (2020) e00152.
[11] P. Xu, Z. Yang, X. Yu, J. Holoubek, H. Gao, M. Li, G. Cai, I. Bloom, H. Liu, Y. Chen, K. An, K.Z. Pupek, P. Liu, Z. Chen, ACS Sustainable Chem. Eng. 9 (2021) 4543–4553.
[12] T. Yang, Y. Lu, L. Li, D. Ge, H. Yang, W. Leng, H. Zhou, X. Han, N. Schmidt, M. Ellis, Z. Li, Adv. Sustainable Syst. 4 (2020) 1900088.
[13] M. Kotobuki, H. Munakata, K. Kanamura, Y. Sato, T. Yoshida, J. Electrochem. Soc. 157 (2010) A1076.
[14] R. Murugan, V. Thangadurai, W. Weppner, Angew. Chem. 46 (2007) 7778–7781.
[15] M. Rosen, R. Ye, M. Mann, S. Lobe, M. Finsterbusch, O. Guillon, D. Fattakhova-Rohlfing, J. Mater. Chem. A 9 (2021) 4831–4840.
[16] R. Ye, C.-L. Tsai, M. Ihrig, S. Sevinc, M. Rosen, E. Dashjav, Y.J. Sohn, E. Figgemeier, M. Finsterbusch, Green Chem. 22 (2020) 4952–4961.
[17] R.-H. Shin, S. Son, S.-S. Ryu, H.-T. Kim, Y.-S. Han, J. Korean Powder Metall. Inst. 23 (2016) 379–383.
[18] K. Gao, M. He, Y. Li, Y. Zhang, J. Gao, X. Li, Z. Cui, Z. Zhan, T. Zhang, J. Alloys Compd. 791 (2019) 923–928.
[19] R.A. Jonson, P.J. McGinn, Solid State Ionics 323 (2018) 49–55.
[20] Z. Fu, L. Zhang, J.E. Gritton, G. Godbey, T. Hamann, Y. Gong, D. McOwen, E. Wachsman, ACS Appl. Mater. Interfaces 12 (2020) 24693–24700.
[21] E. Yi, W. Wang, J. Kieffer, R.M. Laine, J. Mater. Chem. A 4 (2016) 12947–12954.
[22] L. Schwich, M. Küpers, M. Finsterbusch, A. Schreiber, D. Fattakhova-Rohlfing, O. Guillon, B. Friedrich, Metals 10 (2020) 1523.
[23] M. Ali Nowroozi, A. Iqbal Waidha, M. Jacob, P.A. van Aken, F. Predel, W. Ensinger, O. Clemens, Chemistry (Rajkot, India) 11 (2022) e202100274.
[24] K. Schneider, V. Kiyek, M. Finsterbusch, B. Yagmurlu, D. Goldmann, Metals 13 (2023) 834.
[25] P. Xu, Q. Dai, H. Gao, H. Liu, M. Zhang, M. Li, Y. Chen, K. An, Y.S. Meng, P. Liu, Y. Li, J.S. Spangenberger, L. Gaines, J. Lu, Z. Chen, Joule 4 (2020) 2609–2626.
[26] Q. Liang, H. Yue, S. Wang, S. Yang, K. Lam, X. Hou, Electrochim. Acta 330 (2020) 135323.
[27] D.H.S. Tan, P. Xu, H. Yang, M. Kim, H. Nguyen, E.A. Wu, J.-M. Doux, A. Banerjee, Y.S. Meng, Z. Chen, MRS Energy & Sustainability 7 (2020).
[28] M. Ihrig, L.-Y. Kuo, S. Lobe, A.M. Laptev, C.-A. Lin, C. Tu, R. Ye, P. Kaghazchi, L. Cressa, S. Eswara, S. Lin, O. Guillon, D. Fattakhova-Rohlfing, M. Finsterbusch, ACS Appl. Mater. Interfaces 15 (2023) 4101–4112.
[29] R. Kun, F. Langer, M. Delle Piane, S. Ohno, W.G. Zeier, M. Gockeln, L. Colombi Ciacchi, M. Busse, I. Fekete, ACS Appl. Mater. Interfaces 10 (2018) 37188–37197.
[30] M. Rawlence, I. Garbayo, S. Buecheler, J.L.M. Rupp, Nanoscale 8 (2016) 14746–14753.
[31] A. Paolella, W. Zhu, G. Bertoni, S. Savoie, Z. Feng, H. Demers, V. Gariepy, G. Girard, E. Rivard, N. Delaporte, A. Guerfi, H. Lorrmann, C. George, K. Zaghib, ACS Appl. Energy Mater. 3 (2020) 3415–3424.
[32] L. Cheng, E.J. Crumlin, W. Chen, R. Qiao, H. Hou, S. Franz Lux, V. Zorba, R. Russo, R. Kostecki, Z. Liu, K. Persson, W. Yang, J. Cabana, T. Richardson, G. Chen, M. Doeff, Phys. Chem. Chem. Phys. : Phys. Chem. Chem. Phys. 16 (2014) 18294–18300.
[33] J. Schindelin, I. Arganda-Carreras, E. Frise, V. Kaynig, M. Longair, T. Pietzsch, S. Preibisch, C. Rueden, S. Saalfeld, B. Schmid, J.-Y. Tinevez, D.J. White, V. Hartenstein, K. Eliceiri, P. Tomancak, A. Cardona, Nat. Methods 9 (2012) 676–682.
[34] L. Cheng, M. Liu, A. Mehta, H. Xin, F. Lin, K. Persson, G. Chen, E.J. Crumlin, M. Doeff, ACS Appl. Energy Mater. 1 (2018) 7244–7252.
[35] M. Ihrig, M. Finsterbusch, C.-L. Tsai, A.M. Laptev, C. Tu, M. Bram, Y.J. Sohn, R. Ye, S. Sevinc, S. Lin, D. Fattakhova-Rohlfing, O. Guillon, J. Power Sources 482 (2021) 228905.
[36] M. Mann, M. Küpers, G. Häuschen, M. Finsterbusch, D. Fattakhova-Rohlfing, O. Guillon, Ionics 28 (2022) 53–62.
[37] M. Mann, C. Schwab, M. Ihrig, M. Finsterbusch, M. Martin, O. Guillon, D. Fattakhova-Rohlfing, J. Electrochem. Soc. 169 (2022) 40564.
[38] J. Neises, W.S. Scheld, A.-R. Seok, S. Lobe, M. Finsterbusch, S. Uhlenbruck, R. Schmechel, N. Benson, J. Mater. Chem. A 10 (2022) 12177–12186.
[39] R.P. Rao, W. Gu, N. Sharma, V.K. Peterson, M. Avdeev, S. Adams, Chem. Mater. 27 (2015) 2903–2910.
[40] Y. Chen, E. Rangasamy, C.R. dela Cruz, C. Liang, K. An, J. Mater. Chem. A 3 (2015) 22868–22876.
[41] T.F. Malkowski, E.D. Boeding, D. Fattakhova-Rohlfing, N. Wettengl, M. Finsterbusch, G.M. Veith, Ionics 28 (2022) 3223–3231.
[42] J. Awaka, A. Takashima, K. Kataoka, N. Kijima, Y. Idemoto, J. Akimoto, Chem. Lett. 40 (2011) 60–62.
[43] C.-L. Tsai, V. Roddatis, C.V. Chandran, Q. Ma, S. Uhlenbruck, M. Bram, P. Heitjans, O. Guillon, ACS Appl. Mater. Interfaces 8 (2016) 10617–10626.